IEEE Access
Multidisciplinary | Rapid Review | Open Access Journal

Received April 11, 2019, accepted April 29, 2019, date of publication May 2, 2019, date of current version May 17, 2019.

Digital Object Identifier 10.1109/ACCESS.2019.2914466

Control of Multiple Fano Resonances Based on a Subwavelength MIM Coupled Cavities System

ZHENGFENG LI, KUNHUA WEN, LI CHEN, LIANG LEI, JINYUN ZHOU, DONGYUE ZHOU, YIHONG FANG, AND BINGYE WU

School of Physics and Optoelectronic Engineering, Guangdong University of Technology, Guangzhou 510006, China

Corresponding author: Kunhua Wen (khwen@gdut.edu.cn)

This work was supported in part by the Science and Technology Project of Guangzhou under Grant 201904010243, in part by the National Natural Science Foundation of China under Grant 61405039 and Grant 61475037, in part by the Science and Technology Planning Projects of Guangdong Province, China, under Grant 2016A020223013, in part by the Natural Science Foundation of Guangdong Province, China, under Grant 2014A030310300, in part by the State Key Lab of Optical Technologies for Micro-Engineering and Nano-Fabrication of China, in part by the Foundation for Distinguished Young Talents in Higher Education of Guangdong, China, under Grant 2014KQNCX066, and in part by the Research Fund of Guangdong University of Technology under Grant 16ZK0041 and Grant 13ZK0387.

ABSTRACT In this paper, we investigate and analyze numerically and theoretically a coupled plasmonic resonant system by using finite-difference time-domain (FDTD) method and multimode interference coupled-mode theory (MICMT), respectively. First, by employing an end-coupled cavity associated with two side-coupled cavities, three ultra-sharp and asymmetrical Fano resonant peaks are observed in the transmission spectrum. High refractive index sensitivities and high figure of merits are achieved for all the peaks. In the interest of highly integrated optical devices, up to seven Fano peaks with asymmetrical line shapes are achieved when the composite structure is successfully extended by two additional cavities, whereas most of the reported results are about 1–4 Fano resonances in a single structure. Preferred performances are also obtained for this chip-scale structure. This proposed structure may have great potential applications for on-chip optical sensing and optical communication in highly integrated photonic circuits.

INDEX TERMS Metal-insulator-metal waveguides, Fano resonance, plasmonic structure, surface plasmon polaritons (SPPs).

I. INTRODUCTION

Fano resonance emerges from the coherent interference between a localized state and a continuous state in quantum system [1]–[4]. Unlike the Lorentz resonance, Fano resonance exhibits an ultra-sharp and asymmetric line shape with properties of high refractive-index sensitivity (S), high figure of merit (FOM), and strong field enhancements. These unique characteristics allow Fano resonances to be applied in various fields, such as bio-chemical sensing [3], [5], optical switching [6], [7] and fast light or slow light devices [8], [9]. As electron-beam lithography develops rapidly in recent years, nano-scale metal-insulator-metal (MIM) waveguide structures, which are preferred in the realization of highly integrated optical circuits, have drawn many researchers' attention. This is benefited from the surface plasmon polaritons (SPPs), which can overcome the diffraction limit of light and confine light in subwavelength dimensions [10]–[16]. Interestingly, the optical behavior of Fano resonance is also observed in MIM-based structure. Consequently, a lot of plasmonic MIM structures with different configurations have been designed to obtain single or dual sharp and asymmetrical Fano resonant peaks from visible to near-infrared wavelength range [17]–[25]. However, in view of the development of highly integrated optical circuits, one should also look forward to exploring the generation of more Fano resonances in single MIM structure due to their parallel processing capability [26]–[28].

In this paper, multiple Fano resonances are theoretically and numerically investigated in an end-coupled cavities system. Firstly, a vertical rectangular cavity is placed between the input and output MIM waveguides, while two identical horizontal rectangular cavities are side coupled to the vertical one above the waveguides. Originating from mode interactions, three Fano resonances with high refractive index sensitivity and high FOM are generated in this basic structure.

The associate editor coordinating the review of this manuscript and approving it for publication was Zeeshan Kaleem.

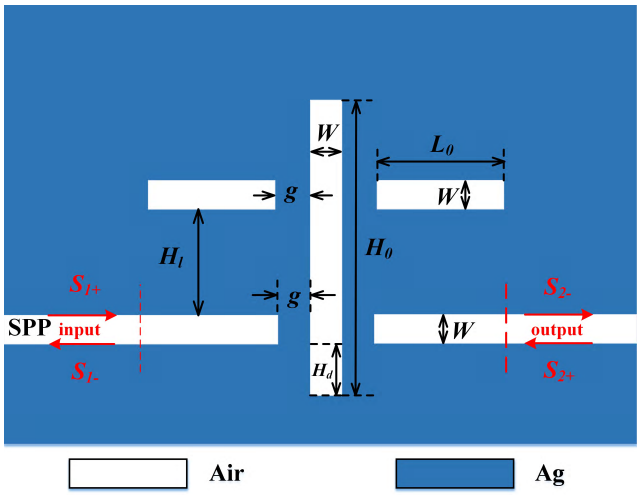

FIGURE 1. Schematic diagram of the basic structure composed of an end-coupled vertical cavity side-coupled by two horizontal cavities.

Moreover, the basic structure is extended by two rectangular cavities, giving rise to seven sharp and asymmetric Fano resonances with excellent performances. The performances of the proposed structure are analyzed by FDTD method and multimode interference coupled mode theory (MICMT), respectively. It is believed that the proposed MIM structure and its diverse configuration options can find more complex applications in highly integrated optical circuits.

II. THEORETICAL ANALYSIS AND SIMULATION RESULTS

The schematic diagram of the proposed structure is shown in Fig. 1. A vertical cavity (called as cavity VC) is perpendicularly set between the input and output MIM waveguides with a coupling distance of $g = 10$nm. Then two identical side-coupled horizontal cavities (called as cavity HC), which are symmetrically distributed on both sides of the vertical one with a coupling distance of $g = 10$nm. These two cavities HC actually can be treated as one cavity for simplicity during the analysis, but dual-cavity-distribution structure can enhance the resonant effect.

For single plasmonic MIM cavity performed as an FP resonator, constructive interference between the resonant modes should occur when the following resonant condition is satisfied: $4\pi Re\left(n_{eff}\right)L/\lambda+\varphi = 2m\pi, m = 1, 2, 3, \ldots$ [29], [30]. Thus, the resonant wavelength can be determined by:

$$\lambda = \frac{2Re\left(n_{eff}\right)L}{m-\varphi/2\pi}, \quad m = 1, 2, 3, \ldots \tag{1}$$

where $Re\left(n_{eff}\right)$ is the real part of the effective refractive index, which can be obtained from the dispersion equations [11], L is the length of the cavity, m stands for the resonant-mode order, and φ is the phase shift caused by the SPP reflection at the cavity facets. Additionally, since the resonant wavelength is proportional to the length of the cavity, the length should be precisely designed to obtain Fano resonance.

Furthermore, it is well known that coupled mode theory (CMT) [31], [32] is quite suitable for analyzing the single mode coupling in the plasmonic resonant system, because the coupling phase between the resonant mode and waveguide can be ignored with an appropriate reference. However, when it comes to multiple modes coupling, such as the proposed structure in Fig. 1, the coupling phase and modulus of each resonant mode is different and all of them will affect the transmission. Consequently, multimode interference coupled mode theory (MICMT) [33] is employed to analyze the transmission spectrum for this proposed structure, and it is given as follows:

$$da_n = \left(-j\omega_n - \frac{1}{\tau_{ni}} - \frac{1}{\tau_{nc1}} - \frac{1}{\tau_{nc2}}\right)a_n + \kappa_{n1}S_{n,1+} + \kappa_{n2}S_{n,2+} \tag{2}$$

$$S_{1-} = -S_{1+} + \sum_n \kappa_{n1}^* a_n, \quad \kappa_{n1} = \sqrt{\frac{2}{\tau_{nc1}}}e^{j\theta_{n1}} \tag{3}$$

$$S_{2-} = -S_{2+} + \sum_n \kappa_{n2}^* a_n, \quad \kappa_{n2} = \sqrt{\frac{2}{\tau_{nc2}}}e^{j(\theta_{n2}-\varphi_n)} \tag{4}$$

$$S_{n,1+} = \gamma_{n1}e^{j\varphi_{n1}}S_{1+}, \quad S_{n,2+} = \gamma_{n2}e^{j\varphi_{n2}}S_{2+} \tag{5}$$

where a_n and ω_n are the normalized amplitude and resonant frequency of the *n-th* resonant mode, respectively. τ_{ni} is the decay time of internal loss of the *n-th* resonant mode in resonator, where as τ_{nc1} and τ_{nc2} are the decay time of the coupling between the resonator and waveguides. $\gamma_{n1}e^{j\varphi_{n1}}$ and $\gamma_{n2}e^{j\varphi_{n2}}$ stand for the normalized coefficients ($\gamma_{n1} = \gamma_{n2} \approx 1$ in this paper). θ_{n1} and θ_{n2} are the coupling phases of the *n-th* resonant mode. φ_n describes the phase difference between the output and input ports of the *n-th* resonant mode.

In Fig. 1, $S_{1,2\pm}$ stands for the normalized amplitudes of SPPs in the input and output MIM waveguides, respectively. Besides, the amplitude S_{2+} can be assumed as zero, because SPPs are supposed to be launched from the left MIM waveguide. Consequently, the amplitude transmission coefficient of this structure is expressed as:

$$t = \frac{S_{2-}}{S_{1+}} = \sum_n \frac{\gamma_{n1}\left|\kappa_{n1}\right|\left|\kappa_{n2}\right|e^{j\phi_n}}{-j\left(\omega-\omega_n\right)+\frac{1}{\tau_{nc1}}+\frac{1}{\tau_{nc2}}+\frac{1}{\tau_{ni}}} \tag{6}$$

where $\phi_n = \varphi_{n1}+\varphi_n+\theta_{n1}-\theta_{n2}$ represents the total coupling phase difference of the *n-th* resonant mode. Since the input and output waveguides are symmetrical to cavity VC and have the uniform width, it can be concluded as $\tau_{nc1} = \tau_{nc2} = \tau_n$ and $\theta_{n1} = \theta_{n2}$, where τ_n is an algebraic value to replace τ_{nc1} and τ_{nc2}. Thus, the transmission T of the structure can be simplified as:

$$T = |t|^2 \approx \left|\sum_n \frac{2e^{j\phi_n}}{-j\left(\omega-\omega_n\right)\tau_n+2+\frac{\tau_n}{\tau_{ni}}}\right|^2 \tag{7}$$

In the following, FDTD method is utilized to investigate the performance of this two-dimensional structure instead of a three-dimension one for saving the hardware resources and the running time, and the accuracy of simulated results

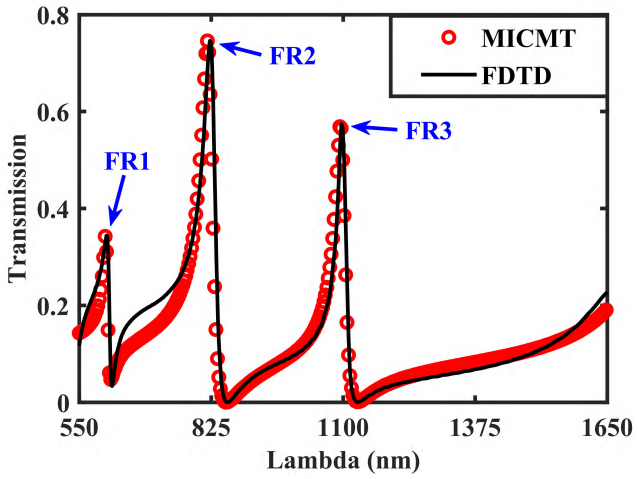

FIGURE 2. Transmission spectra of the basic structure based on FDTD (black solid line) and MICMT (red circle line) methods.

will not be affected. Firstly, we set the metal and insulator as silver (Ag) and air, respectively, and the optical constants of silver are obtained from [34]. The height of cavity VC is $H_0 = 530$nm, and the part below the MIM waveguides is set as $H_d = 30$ nm. The length of the horizontal cavities is $L_0 = 275$nm and their relative height to the waveguides is $H_l = 175$nm. The width of the waveguides and cavities are fixed as $W = 50$nm. The simulated transmission spectrum of the proposed structure is plotted in Fig. 2 using black solid line. Obviously, three asymmetrical Fano resonant peaks (marked as FR1, FR2 and FR3, respectively) emerge in the spectrum at $\lambda = 608$nm with a transmittance of $\sim$0.34, $\lambda = 823$nm with a transmittance of $\sim$0.75 and $\lambda = 1099$nm with a transmittance of $\sim$0.57, respectively. The Fano resonances are further investigated by the MICMT method plotted in Fig. 2 using red circle line, which is highly in accordance with the results obtained by FDTD method.

Moreover, we study the transmission spectrum by changing the parameters of the proposed structure. Firstly, the structure without the horizontal cavities, as shown in the inset of Fig. 3(a), is investigated to excavate the effect of the parameter H_d (shaded area of cavity VC) on the spectrum. Evidently, two asymmetrical Fano peaks FR1 and FR2 emerge in the spectrum owing to the broken symmetry of the structure. When cavity VC moves down (i.e. H_d increases)with H_0 remained, FR2 has a blue shift with the asymmetry increasing, while FR1 is influenced a lot. It is because that the asymmetry will affect the differences of the phase delays of SPPs which will propagate from the below part and upper part of cavity VC, respectively. Thus, the interference at cavity VC is changed, leading to different Fano resonant responses. After setting $H_d = 30$nm and adding horizontal cavities with $L_0 = 275$nm, the transmission spectra with different H_0 are plotted in Fig. 3(b). It is obvious that FR1 and FR2 are enhanced by adding cavity HC and according to equation (1), the effective length of cavity HC increase as H_0 increases so that the resonant wavelengths of all modes move to the long wavelength range. The lengths of the horizontal cavities are also changed to investigate their influences on Fano resonances. In Fig. 3(c), the length L_0 increases from 275nm to 325nm, while H_0 and H_d remains 530nm and 30nm, respectively. It can be observed that similar wavelength variations for Fano resonances are realized in this case. However, the transmittance of FR3 declines a lot owing to the total coupling phase difference ϕ_n, which is attributed to the mode in the cavity HC being changed with the length of the cavity. Thus, the transmittance of FR3 changes correspondingly based on equation (7).

More details of physical mechanism for Fano resonances are exhibited through magnetic field distributions in Fig. 4(a)-(f) corresponding to the Fano resonant peaks at 608 nm, 823 nm and 1099 nm, respectively, and the dips at 617nm, 860nm and 1130nm, respectively. It is obviously observed that most of SPPs at the resonant peak wavelengths can propagate from the coupled system to the output port but the ones are prohibited in output port at dips. Corresponding to FR1 and FR2, strong energy is confirmed in asymmetrical cavities, leading to the enhancements for resonances FR1 and FR2. However, Fig. 4(c) indicates that positive energy is contributed in cavity VC at joint J, while negative one is confirmed in cavity HC. Thus, the bright mode supported by cavity VC has an anti-phase difference with the dark mode supported by cavity HC, which will result in destructive interference between these two modes to generate FR3.

To get more insight to the physical characters of Fano resonances, the phase responses and group delays within the resonant windows are also investigated and plotted in Fig. 5(a). The delay time τ can be decided by a formula relational to the phase shift θ: $\tau(\lambda) = -\lambda^2 d\theta/2\pi c d\lambda$ [8], [9], where c is the velocity of light. It can be clearly observed that phase shifts arise around the Fano resonant windows. Correspondingly, positive or negative group delays are available with the maximum values of $\sim$0.14, $\sim$0.08 and $\sim$0.08 ps for three peaks, while ~-0.15, ~-0.43, ~-0.22 ps for three dips, respectively. It is believed that these outstanding features of Fano resonances can be applied in fast light or slow light technologies.

Next, three important factors, i.e. sensitivity, asymmetry degree and figure of merit (FOM), are employed to evaluate the performances of Fano resonances. The refractive index sensitivity (nm/RIU) is defined as $S = \Delta\lambda/\Delta n$, where Δn is the refractive index change and $\Delta\lambda$ is the resonant wavelength shift due to the refractive index change. For convenience of intuitive observation and explanation, a step of 0.1 of refractive index is employed. When the refractive index (n) of the cavities increases from 1.0 to 1.1, the three Fano peaks have a redshift, as shown in Fig. 5(b). Accordingly, the calculated sensitivities of these Fano peaks are 536 nm/RIU, 828 nm/RIU and 1011 nm/RIU, respectively.

Another evaluated factor is the degree of the spectral asymmetry F, defined as the ratio of the wavelengths corresponding to high/low frequency transmission bandwidths (peak to node):$F = \lambda_{high}/\lambda_{low}$ [22], [35], as indicated in Fig. 5(b).

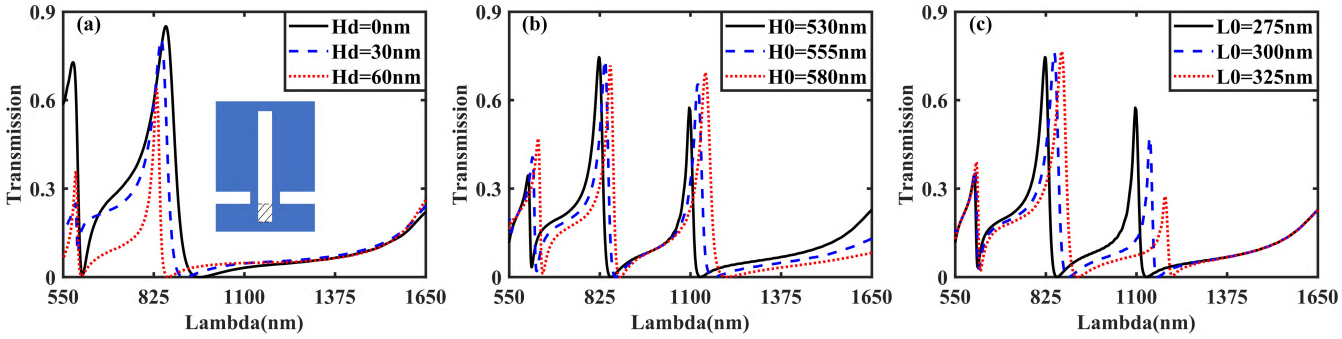

FIGURE 3. The transmission spectra responses for the parameters of the proposed structure, (a) different H_d with $H_0 = 530$nm, (b) different H_0 with $H_d = 30$nm and $L_0 = 275$nm, and (c) different L_0 with $H_d = 30$nm and $H_0 = 530$nm.

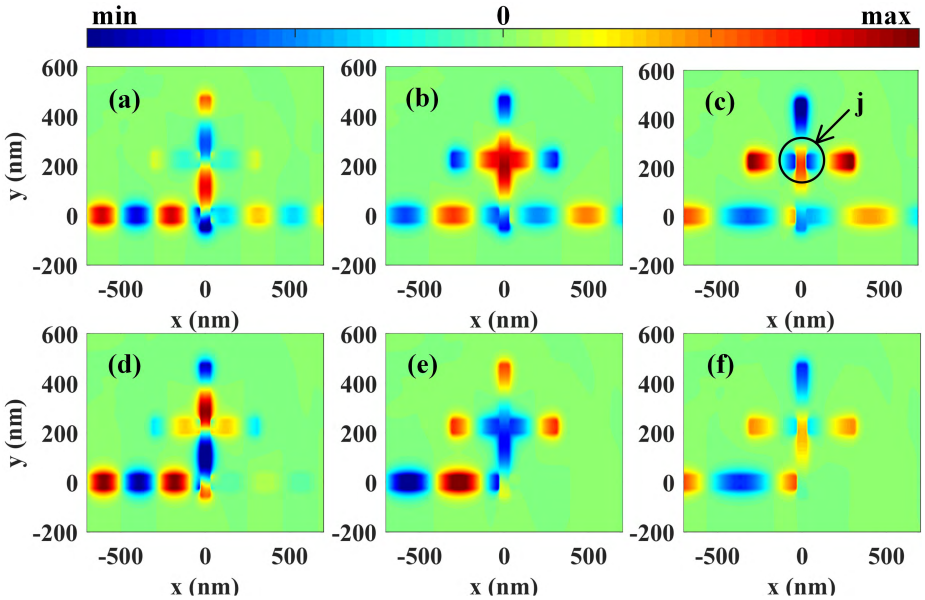

FIGURE 4. (a)-(f) The magnetic field distribution of the proposed structure at peak- or dip-wavelengths of 608 nm, 823 nm, 1099 nm, 617 nm, 860 nm, and 1130 nm, respectively.

FR2 and FR3 possess the ultra-high degree of asymmetry F of 5.7 and 7.9, respectively, meaning that they can be extremely preferred in the sensing and detection areas. In fact, the wavelengths of the bright mode and the dark mode related to the parameters of cavity VC and HC can be precisely designed to achieve the maximum asymmetry of the resonances.

The third important factor in the sensing applications is the figure of merit (FOM), which is expressed as $FOM = 10\lg(\max(\Delta T/\Delta n/T))$, where T is the transmittance at a fixed wavelength and $\Delta T/\Delta n$ is the transmittance change at a fixed wavelength due to the refractive index change. In order to get the maximum FOM, it usually sets the fixed wavelength at ultra-high peak or ultra-low dip. Figure 5(c) shows the calculated FOMs of three Fano peaks. The maximum values of FOMs for three Fano peaks are 29.33 dB, 47.91 dB and 45.31 dB, respectively.

Furthermore, considering the development of photonic integrated circuits, it is preferred to generate more Fano resonances in single structure. According to the analysis above, it is known that Fano resonances originate from mode interactions between the cavities HC and VC, thus the channels of Fano resonances can be flexibly manipulated by extending the proposed structure. One of the effective approaches is to design additional cavities, which can support properly dark modes or bright modes to interact with the ones from the cavities HC or VC, respectively. Considering the integration level and overall performance of multi-process integrated photonic devices, we have designed several configurations to generate more Fano resonances with appropriate transmission intensities and asymmetries after a lot of simulated optimizations. Consequently, as shown in Fig. 6(a), an additional horizontal cavity (called as cavity AHC) is added above cavity VC with a length of $L_c = 500$nm, a width of $W = 50$nm, and a coupling distance of $g = 10$nm. The bottom of cavity AHC is aligned with the left side of cavity VC, i.e. the relative distance between the centers of them is $d = 225$nm. Owing to the mode interferences between the bright mode of cavity VC and dark modes of cavity AHC, dual new Fano peaks emerge

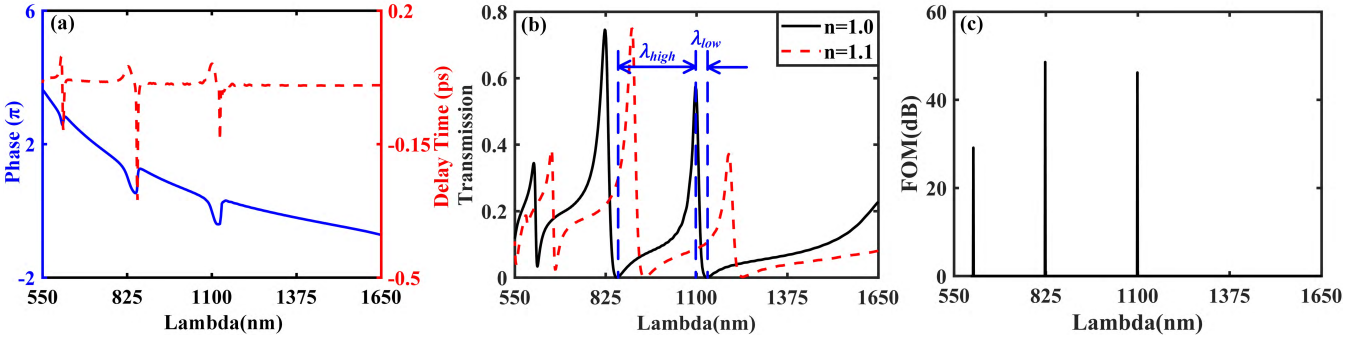

FIGURE 5. (a) Variations of the phase (blue solid line) and the delay times (red dashed line) with respect to the wavelengths for the basic structure. (b) Transmission spectra of the basic structure for different refractive index of the insulator in cavities, $n = 1.0$ (black solid line) and $n = 1.1$ (red dashed line), respectively. (c) FOMs values of the Fano peaks in the basic structure.

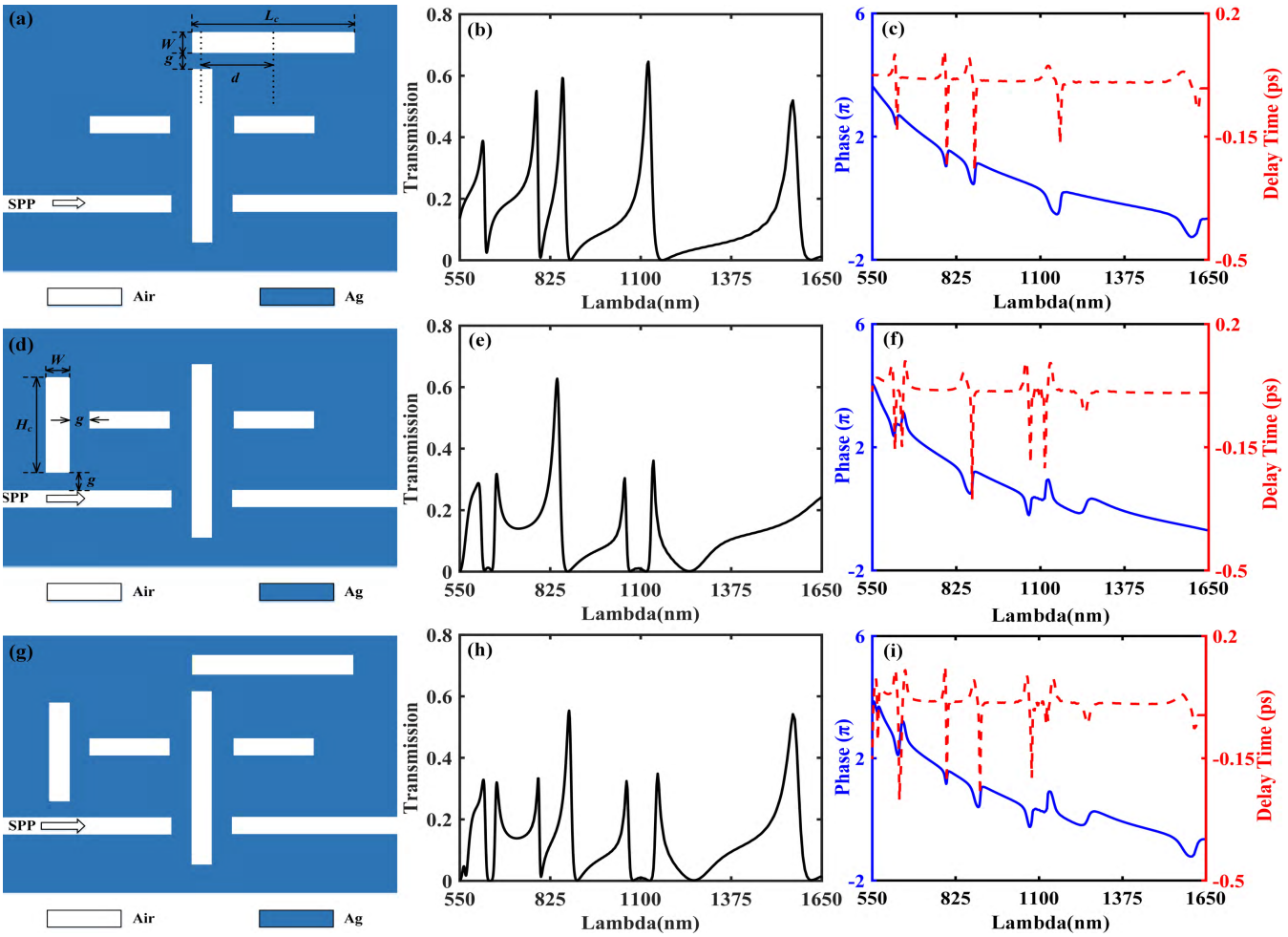

FIGURE 6. (a), (d), and (g) Schematic diagram of the extended structures. (b), (e), and (h) Transmission spectra for the extended structures. (c), (f), and (i) Phase responses (blue solid line) and delay times (red dashed line) for the extended structures.

in the spectrum at $\lambda = 783$nm with a transmittance of $\sim$0.55 and $\lambda = 1562$ nm with a transmittance of $\sim$0.48, respectively, while the original Fano peaks have a redshift, as plotted in Fig. 6(b). Phase perturbations around all the Fano resonant windows are displayed in Fig. 6(c) with blue solid line and corresponding positive or negative group delays are available, illustrating in red dashed line. In another case, the proposed structure can also be extended by setting an additional vertical cavity (called as cavity AVC) at the left side of cavity HC, replacing the cavity AHC, as shown in Fig. 6(d). The cavity AVC is with a height of $H_c = 340$nm, a width of $W = 50$nm, and coupling distance between cavity

TABLE 1. Performances of fano resonances for compact structure with two additional cavities.

Fano peaks(nm)	622	662	789	883	1058	1153	1562
S(nm/RIU)	571	495	777	796	1016	1055	1382
FOM (dB)	48.6	38.4	35.1	44.7	41.5	41.8	35.3

AVC and cavity HC or waveguide of $g = 10$nm. Since SPPs have more paths to cause interferences, five Fano resonances arise in the spectrum in Fig. 6(e). Similar phase responses and group delays around the resonant windows to the cases with cavity AHC are indicated in Fig. 6(f), revealing the features of Fano resonances.

Moreover, in order to enhance the integration level of the device, we take combination with the above two configurations to fabricate a compact structure, of which the schematic diagram is displayed in Fig. 6(g). This would be an effective way to synthetize the spectra in Figs. 6(b) and 6(e) to be a complete one. While keeping the parameters identical to that using in Figs. 6(b) and 6(e), the transmission is shown in Fig. 6(h). As expected, seven Fano resonances are generated in this compact structure, and the spectrum seems to be the perfect synthesis of the spectra in Figs. 6(b) and 6(e). The phase responses and group delays in Fig. 6(i) reveal that seven Fano resonance windows exist simultaneously, which mean it may realize multiple parallel processing functions on a chip. In addition, more details for the performances of Fano resonances in this compact structure are investigated and displayed in Table 1, including the sensitivities and FOMs. Referring to the structure configuration methods of this paper, multi-resonator-coupled system with multiple Fano resonances can be modeled flexibly based on the basic structure to obtain more complex function applications.

III. CONCLUSION

In summary, multiple Fano resonances with 3 to 7 channels have been achieved and investigated in a compact multi-resonator structure. At first, triple Fano resonances are generated in the proposed structure at the wavelengths of 608 nm, 823 nm and 1099 nm, respectively, with a maximum sensitivity of 1011 nm/RIU and a FOM of 47.91 dB. Then the transmission spectral responses with respect to the parameters of cavities VC and HC have also been investigated. Moreover, phase shifts have been achieved in the Fano resonant windows, leading to negative or positive group delays around the dips or peaks, respectively. To meet the requirement of high integrated optical circuits, up to seven Fano resonant peaks are available by adding two additional cavities AHC and AVC. It is believed that this chip-scale plasmonic structure can find important applications in the optical sensing, switching, slow and fast light areas.

ACKNOWLEDGMENT

The authors would like to thank the editor and the reviewers for their valuable comments and suggestions, which help improve the quality of the manuscript.

REFERENCES

[1] U. Fano, "Effects of configuration interaction on intensities and phase shifts," *Phys. Rev.*, vol. 124, no. 6, pp. 1866–1878, Dec. 1961.
[2] A. E. Miroshnichenko, S. Flach, and Y. S. Kivshar, "Fano resonances in nanoscale structures," *Rev. Mod. Phys.*, vol. 82, no. 3, pp. 2257–2298, Aug. 2010.
[3] B. Luk'yanchuk *et al.*, "The Fano resonance in plasmonic nanostructures and metamaterials," *Nature Mater.*, vol. 9, no. 9, pp. 707–715, Aug. 2010.
[4] M. F. Limonov, M. V. Rybin, A. N. Poddubny, and Y. S. Kivshar, "Fano resonances in photonics," *Nature Photon.*, vol. 11, no. 9, pp. 543–554, Sep. 2017.
[5] H. Lu, X. Liu, D. Mao, and G. Wang, "Plasmonic nanosensor based on Fano resonance in waveguide-coupled resonators," *Opt. Lett.*, vol. 37, no. 18, pp. 3780–3782, Sep. 2012.
[6] H. Lu, X. Liu, L. Wang, Y. Gong, and D. Mao, "Ultrafast all-optical switching in nanoplasmonic waveguide with Kerr nonlinear resonator," *Opt. Express*, vol. 19, no. 4, pp. 2910–2915, Feb. 2011.
[7] M. Heuck, P. T. Kristensen, Y. Elesin, and J. Mørk, "Improved switching using Fano resonances in photonic crystal structures," *Opt. Lett.*, vol. 38, no. 14, pp. 2466–2468, Jul. 2013.
[8] K. Wen, Y. Hu, J. Zhou, L. Lei, J. Li, and Y. Wu, "Plasmonic-induced absorption in an end-coupled metal-insulator-metal resonator structure," *Opt. Mater. Express*, vol. 7, no. 2, pp. 433–443, Feb. 2017.
[9] J.-F. Hu, J. Liu, B. Liu, J. Chen, H.-Q. Liang, and G.-Q. Li, "Plasmon-induced absorption and its applications for fast light and sensing based on double-stub resonators," *Optik*, vol. 159, pp. 254–260, Apr. 2018.
[10] W. L. Barnes, A. Dereux, and T. W. Ebbesen, "Surface plasmon subwavelength optics," *Nature*, vol. 159, no. 6950, pp. 824–830, Aug. 2003.
[11] J. A. Dionne, L. A. Sweatlock, H. A. Atwater, and A. Polman, "Plasmon slot waveguides: Towards chip-scale propagation with subwavelength-scale localization," *Phys. Rev. B, Condens. Matter*, vol. 73, no. 3, Jan. 2006, Art. no. 035407.
[12] X. Luo *et al.*, "High-uniformity multichannel plasmonic filter using linearly lengthened insulators in metal–insulator–metal waveguide," *Opt. Lett.*, vol. 38, no. 9, pp. 1585–1587, May 2013.
[13] B. Q. Zhu and H. K. Tsang, "High coupling efficiency silicon waveguide to metal–insulator–metal waveguide mode converter," *J. Lightw. Technol.*, vol. 34, no. 10, pp. 2467–2472, May 2016.
[14] F. Galvez *et al.*, "Plasmonic nanodevice with magnetic funcionalities: Fabrication and characterization," *Opt. Mater. Express*, vol. 6, no. 10, pp. 3086–3096, Oct. 2016.
[15] K. Wen, Y. Hu, L. Chen, J. Zhou, L. Lei, and Z. Guo, "Fano resonance with ultra-high figure of merits based on plasmonic metal-insulator-metal waveguide," *Plasmonics*, vol. 10, no. 1, pp. 27–32, Feb. 2015.
[16] G. Wang *et al.*, "Fano-resonance-based ultra-high-resolution ratio-metric wavelength monitor on silicon," *Opt. Lett.*, vol. 41, no. 3, pp. 544–547, Feb. 2016.
[17] H.-Q. Liang, B. Liu, J.-F. Hu, and X.-D. He, "High efficiency all-optical plasmonic diode based on a nonlinear side-coupled waveguide–cavity structure with broken symmetry," *Opt. Commun.*, vol. 414, pp. 98–101, May 2018.
[18] B. Sun *et al.*, "Tunable Fano resonance in e-shape plasmonic nanocavities," *J. Phys. Chem. C*, vol. 118, no. 43, pp. 25124–25131, Oct. 2014.
[19] Z. Chen, L. Yu, L. Wang, G. Duan, Y. Zhao, and J. Xiao, "Sharp asymmetric line shapes in a plasmonic waveguide system and its application in nanosensor," *J. Lightw. Technol.*, vol. 33, no. 15, pp. 3250–3253, Aug. 1, 2015.
[20] Z. Chen, J. Chen, L. Yu, and J. H. Xiao, "Sharp trapped resonances by exciting the anti-symmetric waveguide mode in a metal-insulator-metal resonator," *Plasmonics*, vol. 10, no. 1, pp. 131–137, Feb. 2015.
[21] J. Chen, Z. Li, J. Li, and Q. Gong, "Compact and high-resolution plasmonic wavelength demultiplexers based on Fano interference," *Opt. Express*, vol. 19, no. 10, pp. 9976–9985, Sep. 2011.

[22] X. Piao, S. Yu, S. Koo, K. Lee, and N. Park, "Fano-type spectral asymmetry and its control for plasmonic metal-insulator-metal stub structures," *Opt. Express*, vol. 19, no. 11, pp. 10907–10912, 2011.
[23] C. Zhao and Y. Li, "Multiple Fano resonances based on different waveguide modes in a symmetry breaking plasmonic system," *IEEE Photon. J.*, vol. 6, no. 6, Dec. 2014, Art. no. 4802208.
[24] S. Yan, M. Zhang, X. Zhao, Y. Zhang, J. C. Wang, and W. Jin, "Refractive index sensor based on a metal–insulator–metal waveguide coupled with a symmetric structure," *Sensors*, vol. 17, no. 12, Dec. 2017, Art. no. 2879.
[25] R. Zafar, S. Nawaz, G. Singh, A. d'Alessandro, and M. Salim, "Plasmonics-based refractive index sensor for detection of hemoglobin concentration," *IEEE Sensors J.*, vol. 18, no. 11, pp. 4372–4377, Jun. 2018.
[26] Z. Chen, X. Song, G. Duan, L. Wang, and L. Yu, "Multiple Fano resonances control in MIM side-coupled cavities systems," *IEEE Photon. J.*, vol. 7, no. 3, Jun. 2015, Art. no. 2701009.
[27] K. H. Wen, L. Chen, J. Y. Zhou, L. Lei, and Y. H. Fang, "A plasmonic chip-scale refractive index sensor design based on multiple Fano resonances," *Sensors*, vol. 18, no. 10, Oct. 2018, Art. no. 3181.
[28] Z. Guo, K. Wen, Q. Hu, W. Lai, J. Lin, and Y. Fang, "Plasmonic multichannel refractive index sensor based on subwavelength tangent-ring metal–insulator–metal waveguide," *Sensors*, vol. 18, no. 5, May 2018, Art. no. 1348.
[29] Q. Zhang, X.-G. Huang, X.-S. Lin, J. Tao, and X.-P. Jin, "A subwavelength coupler-type MIM optical filter," *Opt. Express*, vol. 17, no. 9, pp. 7549–7555, Apr. 2009.
[30] F. Hu, H. Yi, and Z. Zhou, "Band-pass plasmonic slot filter with band selection and spectrally splitting capabilities," *Opt. Express*, vol. 19, no. 6, pp. 4848–4855, Mar. 2011.
[31] H. Haus and W. P. Huang, "Coupled-mode theory," *Proc. IEEE*, vol. 79, no. 10, pp. 1505–1518, Oct. 1991.
[32] Q. Li, T. Wang, Y. Su, M. Yan, and M. Qiu, "Coupled mode theory analysis of mode-splitting in coupled cavity system," *Opt. Express*, vol. 18, no. 8, pp. 8367–8382, Aug. 2010.
[33] S. Li, Y. Wang, R. Jiao, L. Wang, G. Duan, and L. Yu, "Fano resonances based on multimode and degenerate mode interference in plasmonic resonator system," *Opt. Express*, vol. 25, no. 4, pp. 3525–3533, Feb. 2017.
[34] P. B. Johnson and R. W. Christy, "Optical constants of the noble metals," *Phys. Rev. B, Condens. Matter*, vol. 6, no. 12, pp. 4370–4379, Dec. 1972.
[35] X. Piao, S. Yu, and N. Park, "Control of Fano asymmetry in plasmon induced transparency and its application to plasmonic waveguide modulator," *Opt. Express*, vol. 20, no. 17, pp. 18994–18999, Aug. 2012.